Electronic Supplementary Material (ESI) for Physical Chemistry Chemical Physics.

Supporting Information

Emergent superconductivity in TaO_3 at high pressures

Wenjing Li,[1†] Xing Li,[2†] Xiaohua Zhang,[2] Hong Yu,[1] Fanjunjie Han,[1] Aitor Bergara,[3,4,5,*] Jianyan Lin,[6,*] Jinhui Wu[1] and Guochun Yang[1,2,*]

[1]*Centre for Advanced Optoelectronic Functional Materials Research and Key Laboratory for UV Light-Emitting Materials and Technology of Northeast Normal University, Changchun 130024, China*
[2]*State Key Laboratory of Metastable Materials Science & Technology and Key Laboratory for Microstructural Material Physics of Hebei Province, School of Science, Yanshan University, Qinhuangdao 066004, China*
[3]*Departamento de Física, Universidad del País Vasco-Euskal Herriko Unibertsitatea, UPV/EHU, 48080 Bilbao, Spain*
[4]*Donostia International Physics Center (DIPC), 20018 Donostia, Spain*
[5]*Centro de Física de Materiales CFM, Centro Mixto CSIC-UPV/EHU, 20018 Donostia, Spain*
[6]*College of Physics, Changchun Normal University, Changchun 130032*

[†]These authors contributed equally to this work.
*Corresponding Authors E-mail:yanggc468@nenu.edu.cn; yanggc@ysu.edu.cn

Index **Page**

Computational Details

The structure prediction method was based on a global minimization of free energy surfaces combining *ab initio* total-energy calculations methodology, as implemented in the CALYPSO (Crystal structure AnaLYsis by Particle Swarm Optimization) code.[1, 2] The structures of Ta_xO_y (x = 1 y = 1-5; x = 2 y = 1, 3, 5, 7; x = 3 y = 1) were searched with simulation cell sizes of 1-4 formula units (f.u.) at the selected pressures of 1 atm and 50, 100, 200, 300 GPa. In the first step, random structures with certain symmetry were constructed in which atomic coordinates were generated by the crystallographic symmetry operations. Local optimizations using the VASP code[3] were done with the conjugate gradients method and stopped when the total enthalpy changes became smaller than 1×10^{-5} eV per cell. After processing the first-generation structures, 60% of them with lower enthalpies were selected to construct the next generation structures by PSO (Particle Swarm Optimization). 40% of the structures in the new generation were randomly generated. A structure fingerprinting technique of bond characterization matrix was applied to the generated structures, so that identical structures are strictly forbidden. These procedures significantly enhanced the diversity of the structures, which was crucial for structural global search efficiency. In most cases, structural searching simulations for each calculation were stopped after generating 1000 ~ 1200 structures (e.g., about 20 ~ 30 generations).

To further analyze the structures with higher accuracy, we selected a number of structures with lower enthalpies and performed structural optimization using density functional theory within the generalized gradient approximation[4] as implemented in the VASP code. In all the calculations, the cutoff energy for the expansion of wavefunctions in plane waves was set to 750 eV, and the Monkhorst-Pack k-mesh with a grid spacing of $2\pi \times 0.025$ $Å^{-1}$ was selected to meet well energy convergence within ~1 meV/atom. The electron-ion interaction was described by the projector-augmented-wave potentials with $5s^25p^65d^36s^2$ and $2s^22p^4$ configurations considered as valence electrons for Ta and O atoms, respectively.

In order to further test the reliability of the adopted pseudopotentials for Ta and O, the validity of the projector augmented wave (PAW) pseudopotentials from the VASP library were checked by comparing the calculated Birch-Murnaghan equation of state with those obtained from the full-potential linearized augmented plane-wave method (LAPW, as implemented in WIEN2k).[5] The Birch-Murnaghan equation of states derived from PAW and LAPW methods were almost identical (Fig. S0). Thus, our adopted pseudopotentials were feasible in the range of 0-300 GPa.

The electron-phonon coupling calculations were carried out with the density functional perturbation theory (DFPT) in the QUANTUM ESPRESSO package.[6] We employed the ultrasoft pseudopotentials with $5s^25p^65d^36s^2$ and $2s^22p^4$ as valence electrons for Ta, and O atoms, respectively. The kinetic energy cutoff and width of the Gaussians were chosen as 100 and 0.05 Ry. To reliably calculate electron-phonon coupling in metallic systems, we need to sample dense k-meshes for electronic Brillouin zone integration and enough q-meshes for evaluating average contributions from the phonon modes. Dependent on the specific structures of stable compounds, different k-meshes and q-meshes were used: 10 × 10 × 10 k-meshes and 5 ×5 × 2 q-meshes for TaO_3 in the Pm-3n structure,

16 × 16 × 21 k-meshes and 4 × 4 × 3 q-meshes for TaO_2 in the *I*4/*mmm* structure, 15 × 15 ×6 k-meshes and 5 × 5 × 2 q-meshes for TaO in the $P6_3/mmc$ structure, 6 × 10 × 10 k-meshes and 2 × 5 × 5 q-meshes for Ta_2O in the $P2_1/m$ structure, 8 × 8 × 8 k-meshes and 4 × 4 × 4 q-meshes for TaS_3 and $TaSe_3$ in the *Pm*-3*n* structure. We have calculated the superconducting T_c of Ta-O/S/Se compounds as estimated from the McMillan-Allen-Dynes formula:[7-9]

$$T_c = \frac{\omega_{log}}{1.2} exp\left[-\frac{1.04(1 + \lambda)}{\lambda - \mu^*(1 + 0.62\lambda)} \right].$$

Here, μ^* is the Coulomb pseudopotential (μ^* = 0.1). The electron-phonon coupling constant, λ, and the logarithmic average phonon frequency, ω_{log}, were calculated by the Eliashberg spectral function for electron-phonon interaction:

$$\alpha^2F(\omega) = \frac{1}{N(E_F)} \sum_{kq,v} |g_{k,k+q,v}|^2 \delta(\varepsilon_k)\delta(\varepsilon_{k+q})\delta(\omega - \omega_{q,v}),$$

where $\lambda = 2\int d\omega \frac{\alpha^2F(\omega)}{\omega}$; $\omega_{log} = exp\left[\frac{2}{\lambda}\int \frac{d\omega}{\omega}\alpha^2F(\omega)ln(\omega)\right]$. Herein, $N(E_F)$ is the electronic density of states at the Fermi level, $\omega_{q,v}$ is the phonon frequency of mode v and wave vector q, and $|g_{k,k+q,v}|$ is the electron-phonon matrix element between two electronic states with momenta k and $k + q$ at the Fermi level.[10, 11]

Supporting Figures

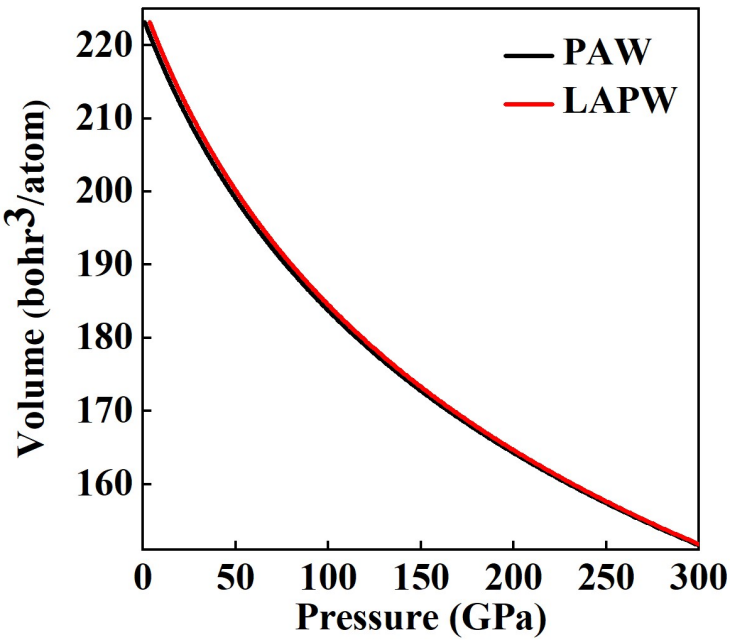

Figure S0. Comparison of the fitted Birch-Murnaghan equation of states for *Pm*-3*n* TaO_3 by using the calculated results with the PAW pseudopotentials and the full-potential LAPW methods.

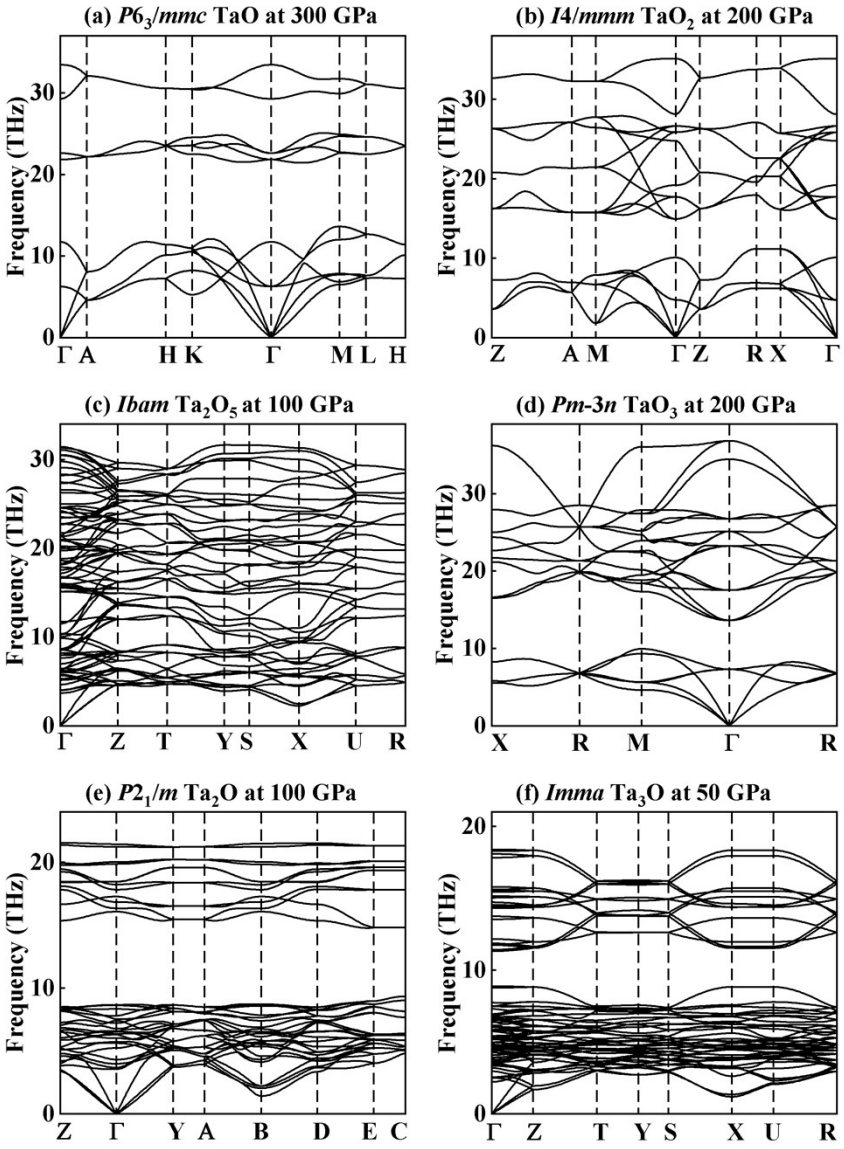

FIG. S1. Phonon dispersion curves of the stable Ta-O phases.

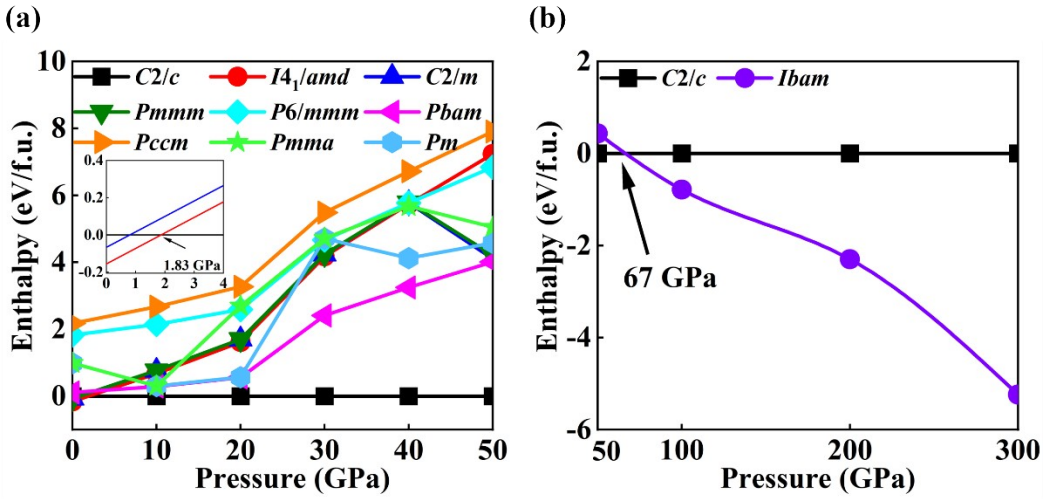

FIG. S2. Calculated enthalpy as a function of pressure for the reported[12-19] and predicted Ta_2O_5 structures relative to the *C*2/*c* phase.

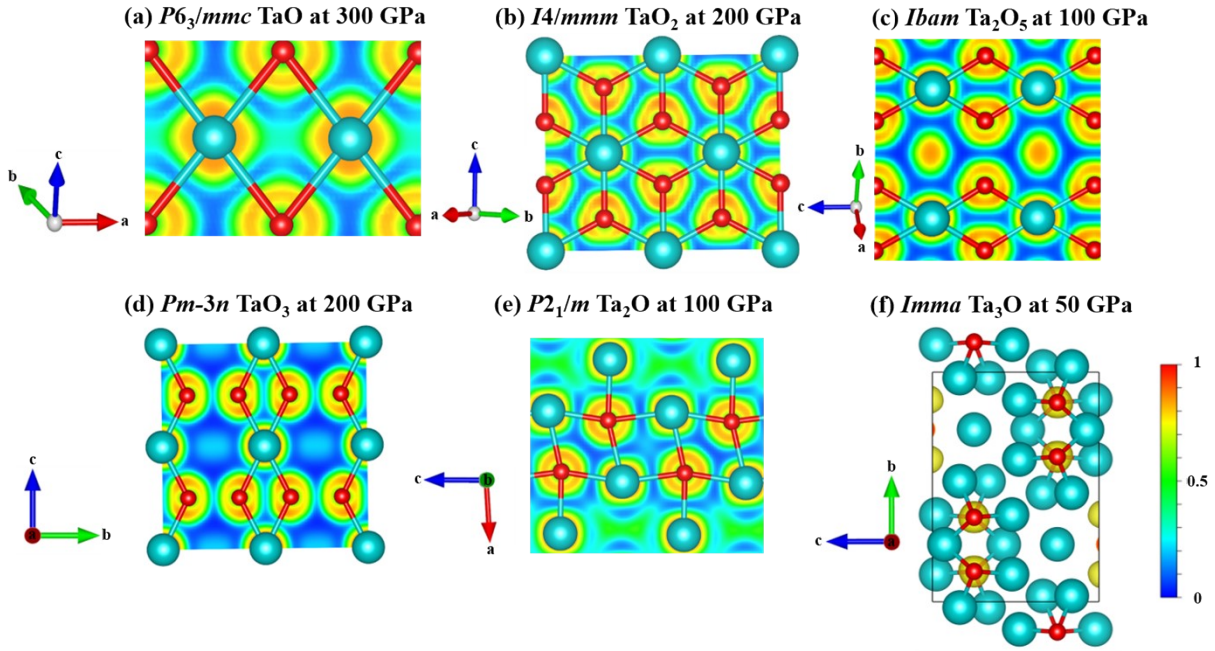

FIG. S3. Electron localization function (ELF) maps of the stable Ta-O phases. The ELF analysis can be used to distinguish different types of chemical bonding.

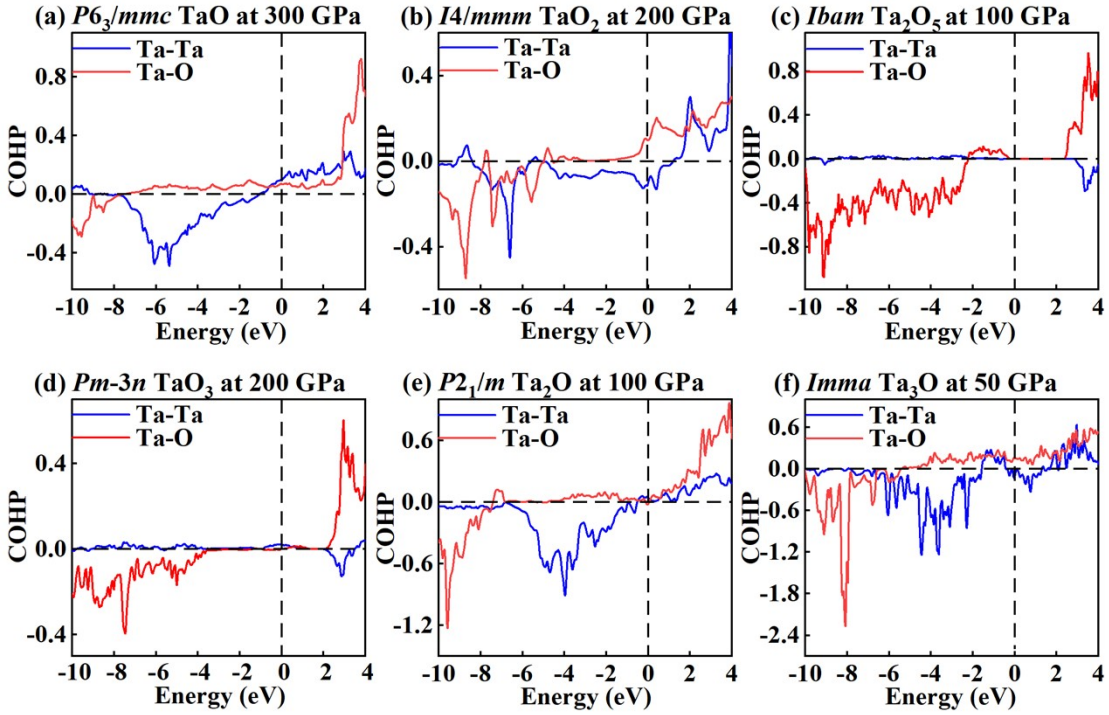

FIG. S4. The crystal orbital Hamiltonian population (COHP) of the Ta-O and Ta-Ta interactions in stable Ta-O compounds. Generally, negative COHP values indicate bonding states, while positive COHP values indicate antibonding states.

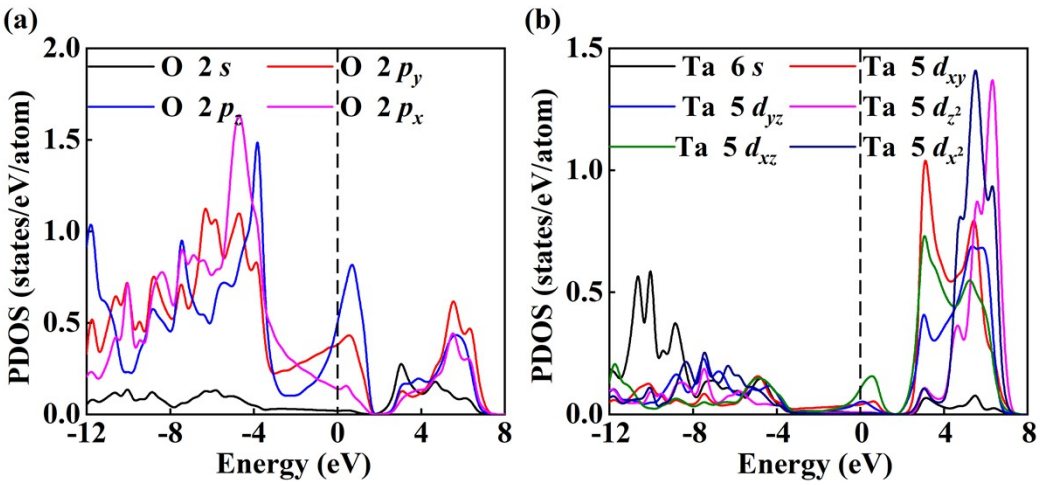

FIG. S5. Projected density of states (PDOS) associated to the (a) O 2*s* and 2*p* orbitals, and (b) Ta 6*s* and 5*d* orbitals in *Pm*-3*n* TaO_3 at 200 GPa.

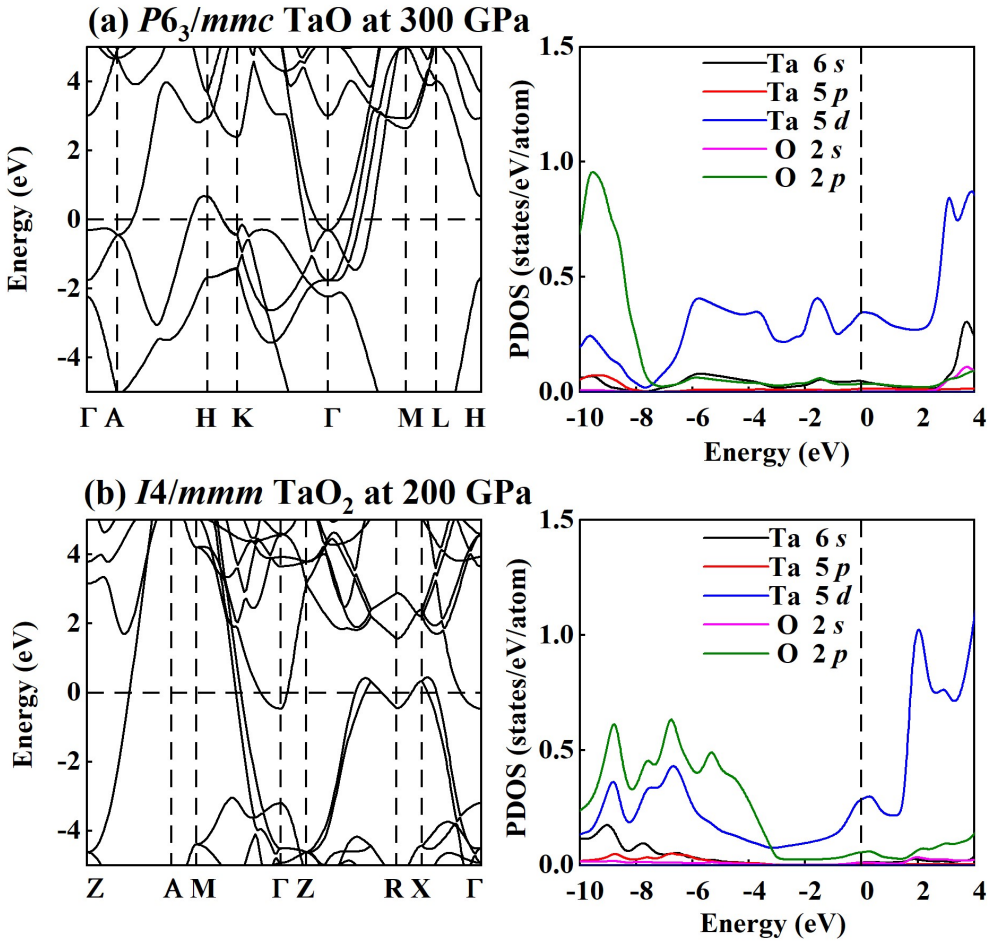

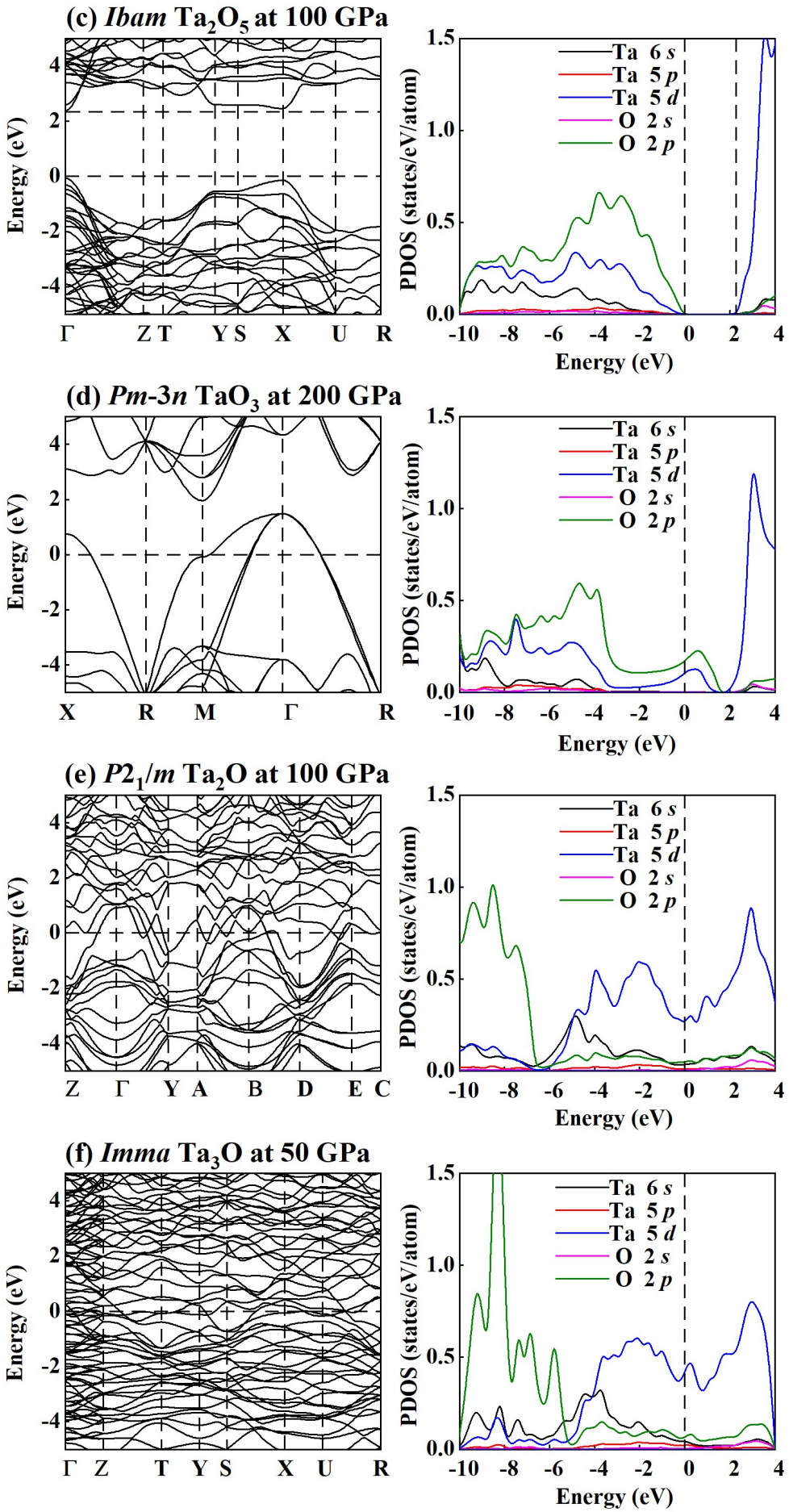

FIG. S6. Electronic band structures and PDOS of the stable Ta-O compounds.

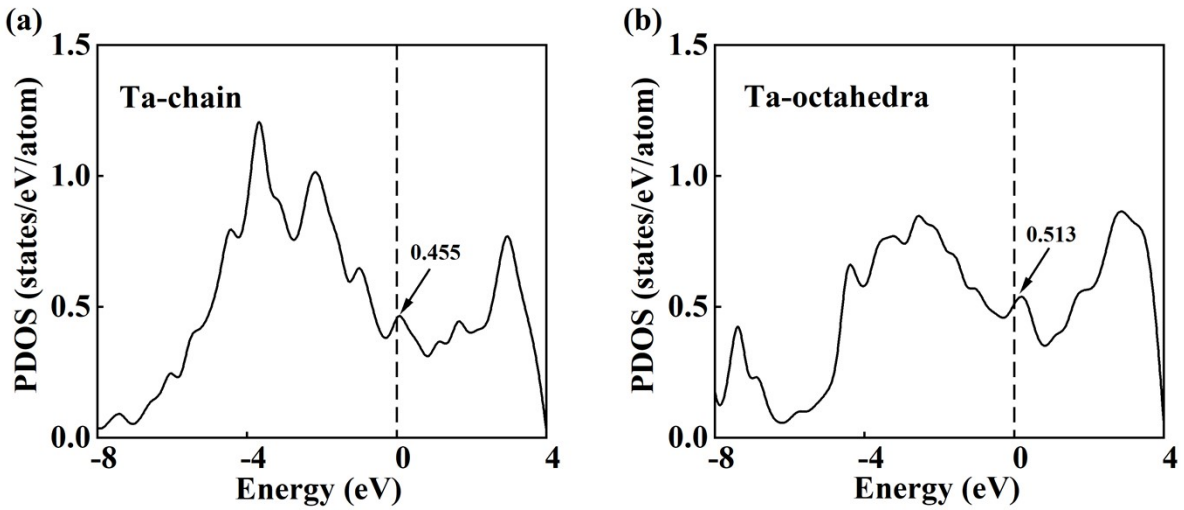

FIG. S7. PDOS of (a) Ta atom forming a linear atomic chain, and (b) Ta atom located in the octahedra in *Imma* Ta_3O at 50 GPa

The electronic density of states (DOS) of the Ta atom forming a linear atomic chain is 0.455 states/eV/atom at the Fermi level, while the DOS of the Ta atom located in the Ta-O octahedra is 0.513 states/eV/atom, showing a greater contribution to the metallicity of Ta_3O.

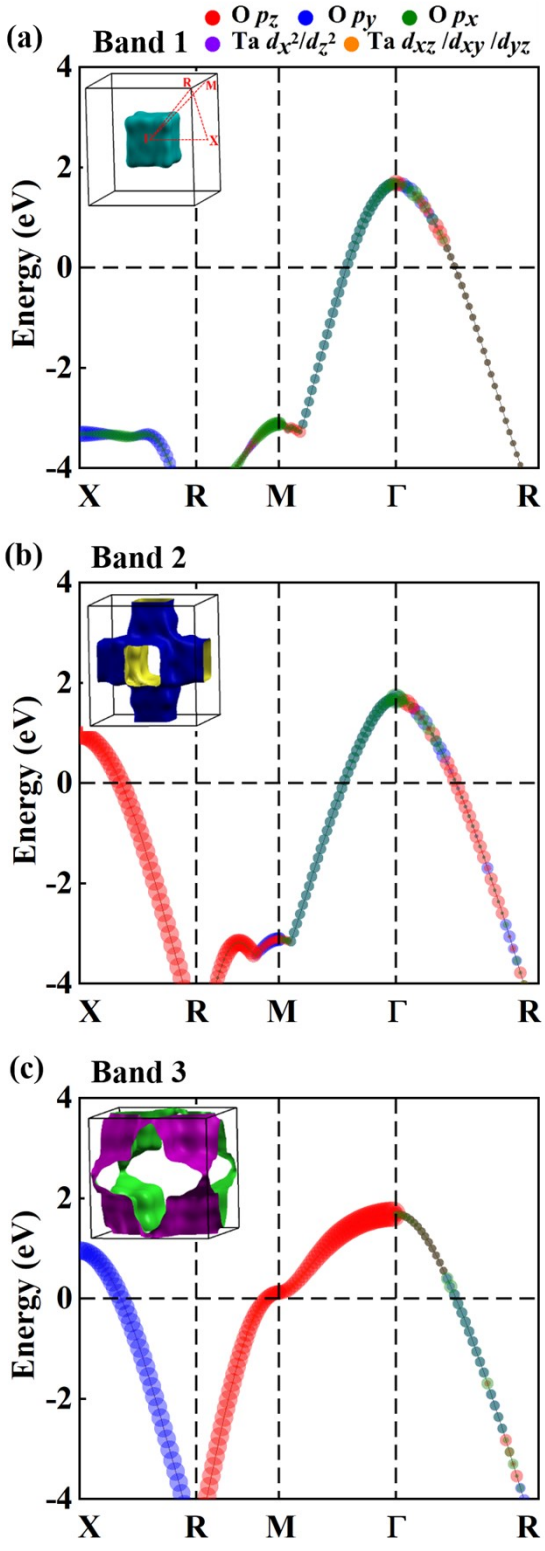

FIG. S8. The first, second, and third bands of *Pm*-3*n* TaO_3 passing through the E_F at 200 GPa.

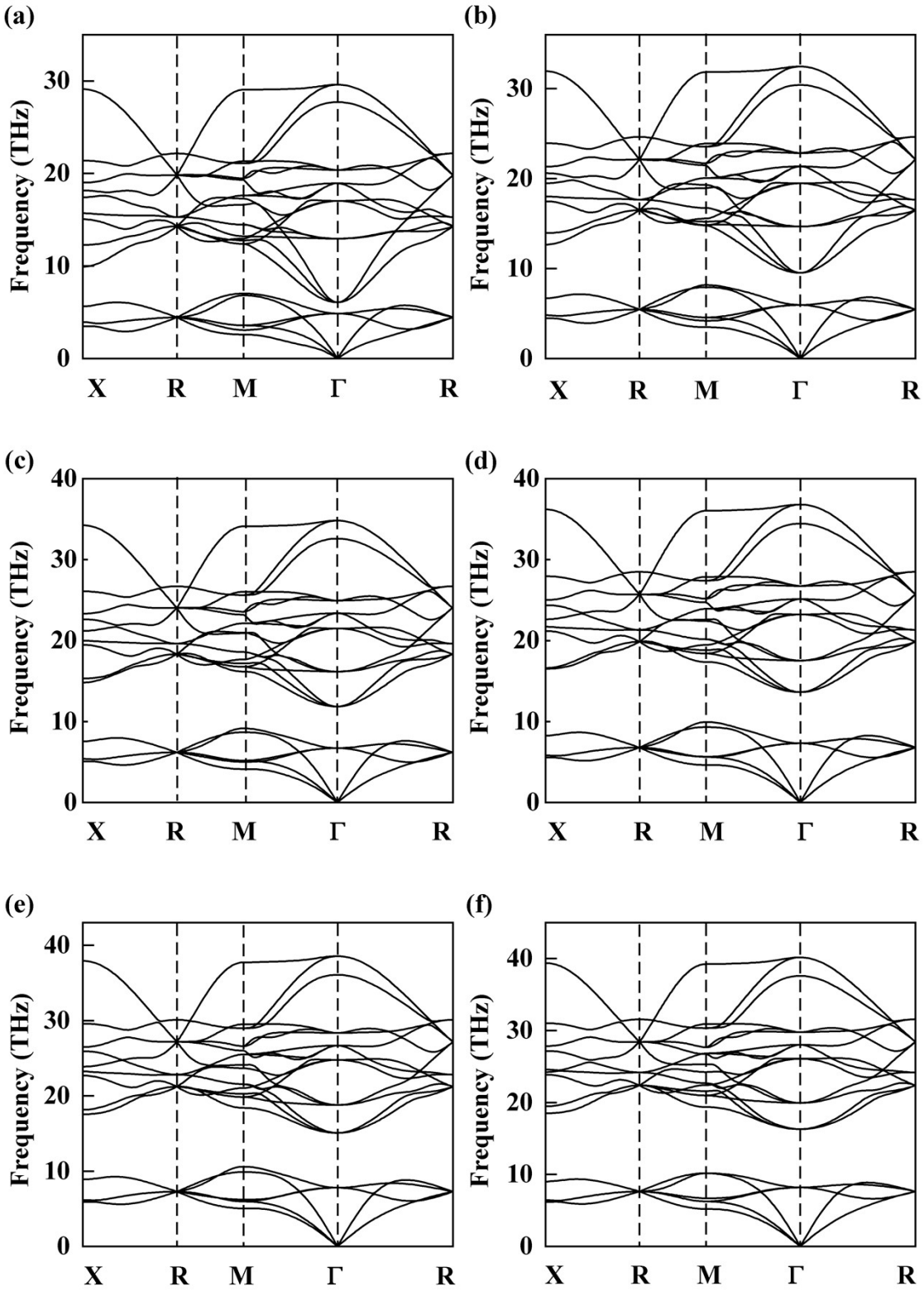

FIG. S9. Phonon dispersion curves of *Pm*-3*n* TaO_3 at (a) 50, (b) 100, (c) 150, (d) 200, (e) 250, and (f) 300 GPa.

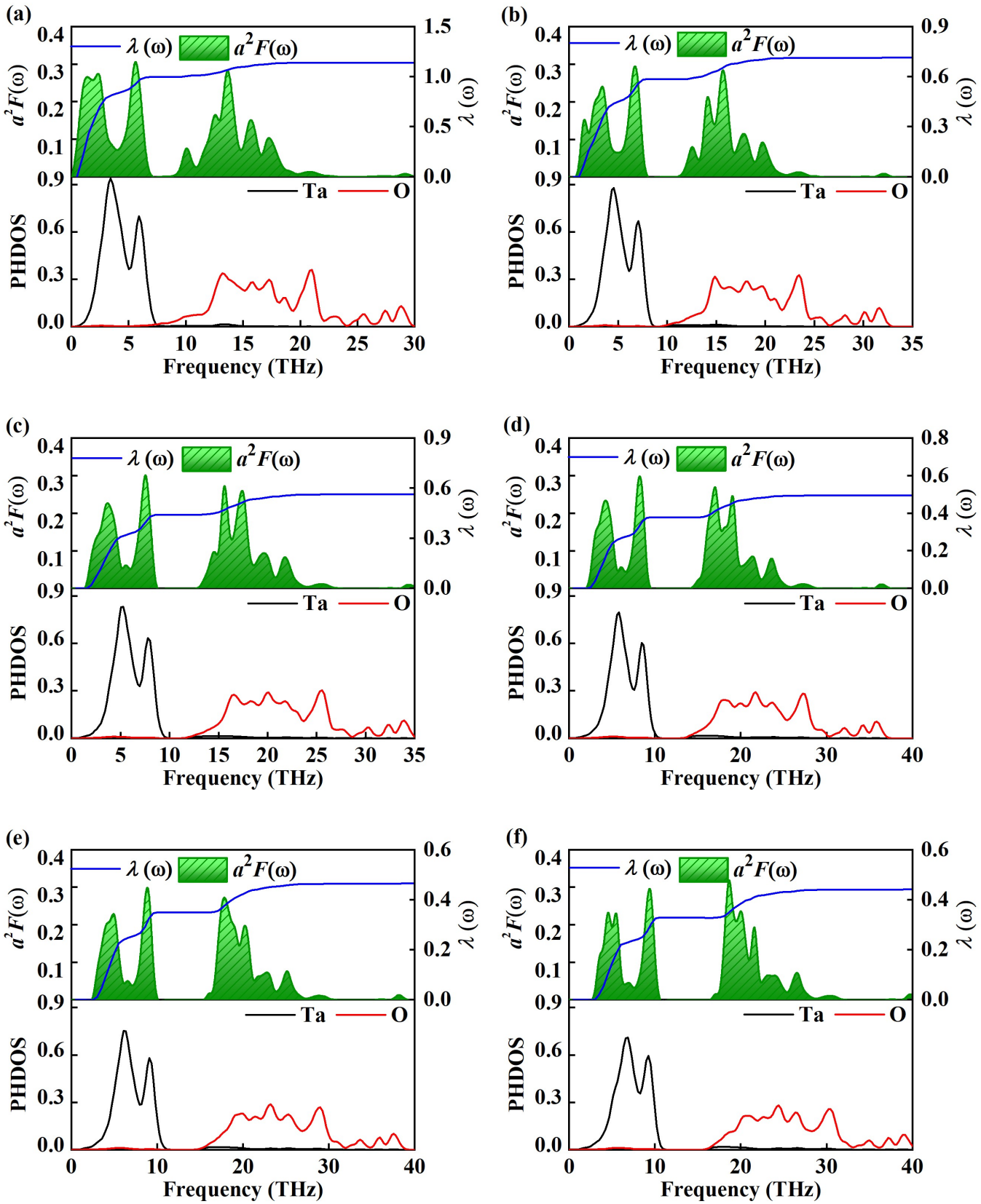

FIG. S10. The projected phonon densities of states (PHDOS) and Eliashberg spectral function of *Pm*-3*n* TaO_3 (a) 50, (b) 100, (c) 150, (d) 200, (e) 250, and (f) 300 GPa.

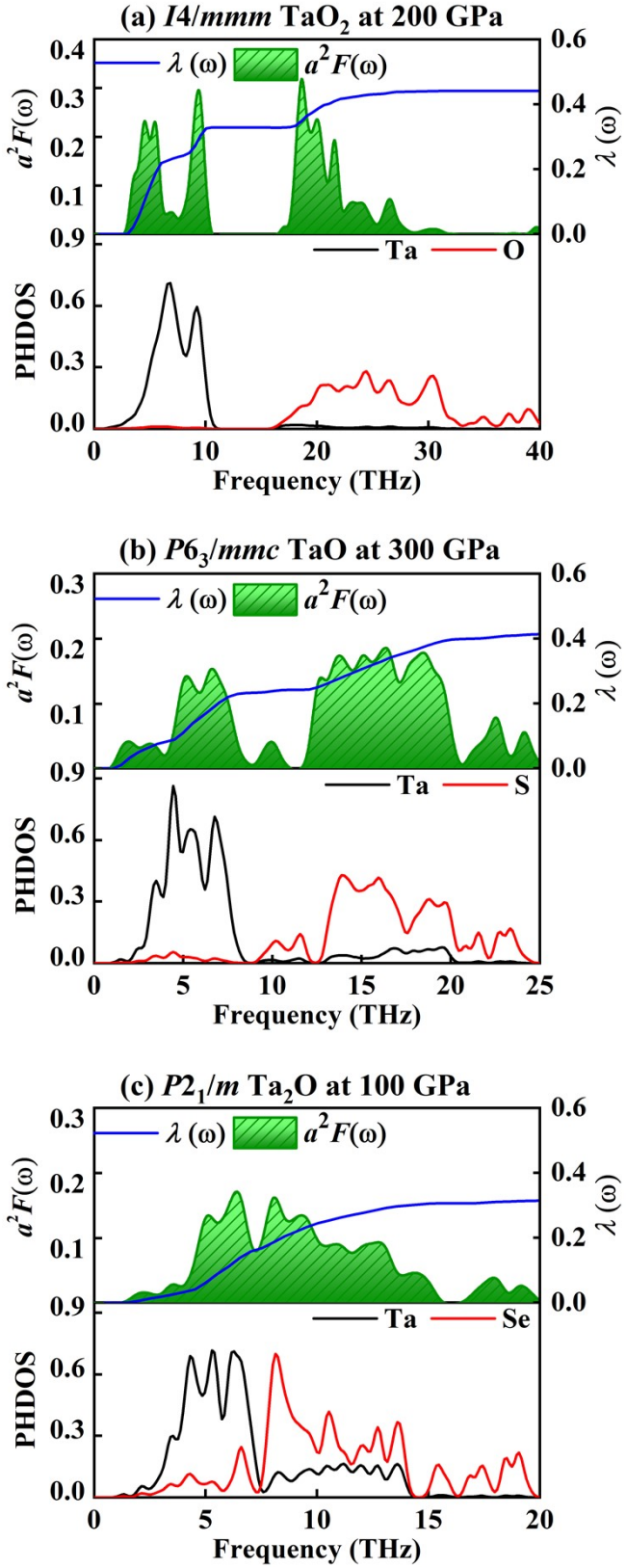

FIG. S11. The PHDOS and Eliashberg spectral functions of (a) *I*4/*mmm* TaO_2 at 200 GPa, (b) *P*6_3/*mmc* TaO at 300 GPa, and (c) *P*2_1/*m* Ta_2O at 100 GPa.

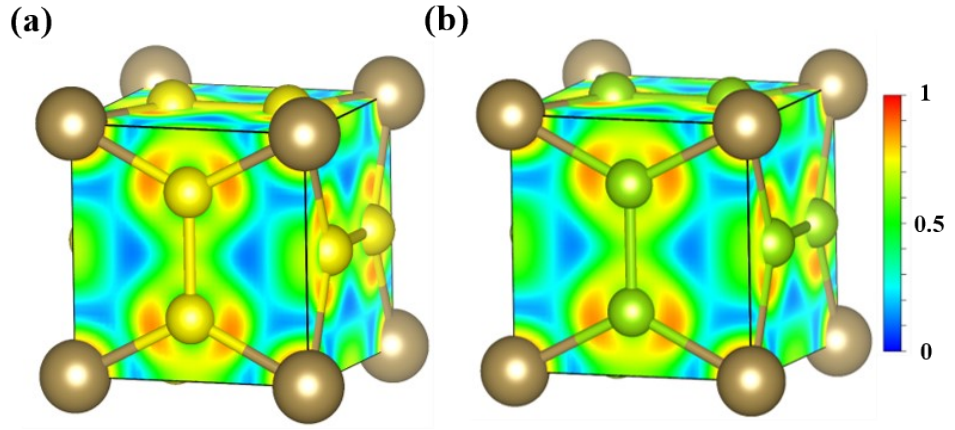

FIG. S12. The ELF maps of (a) *Pm*-3*n* TaS_3 and (b) *Pm*-3*n* $TaSe_3$ at 300 GPa. Golden, yellow, and green spheres represent Ta, S, and Se atoms, respectively.

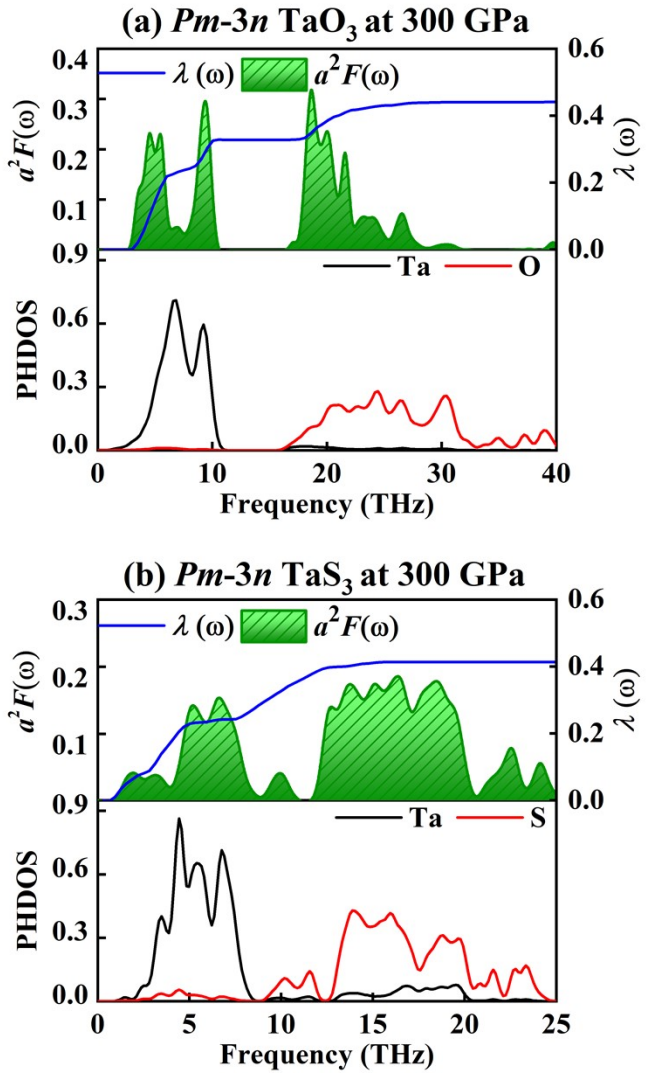

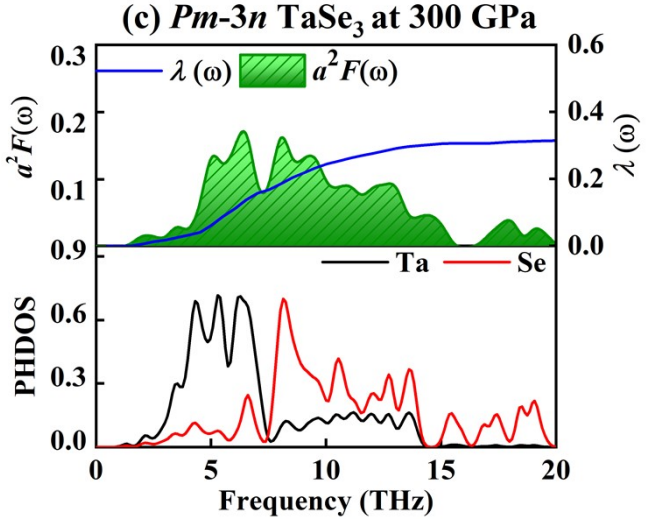

FIG. S13. The PHDOS and Eliashberg spectral functions of *Pm*-3*n* TaX_3 (X = O, S, and Se) at 300 GPa.

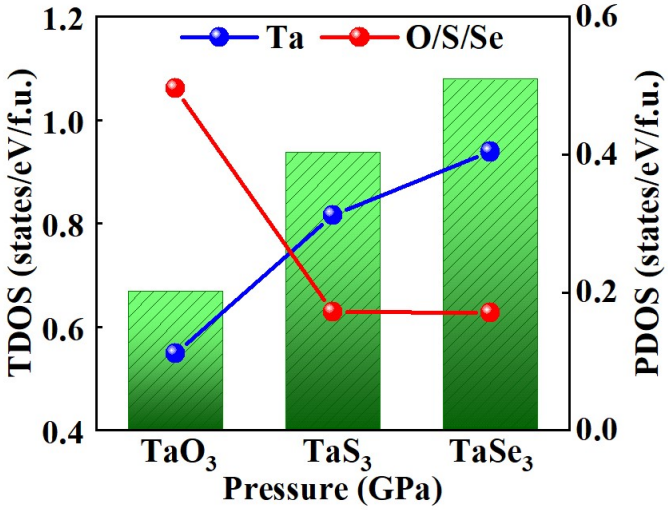

FIG. S14. The total DOS and PDOS of *Pm*-3*n* TaX_3 (X = O, S, and Se) at 300GPa.

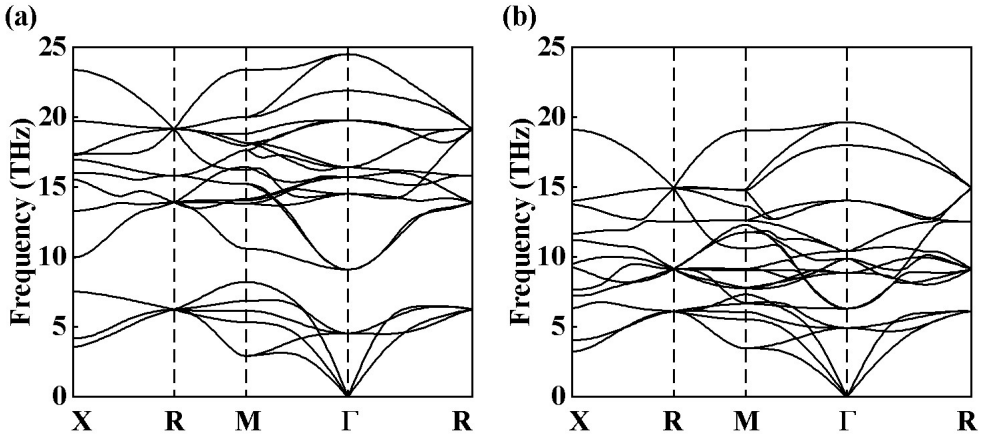

FIG. S15. Phonon dispersion curves of *Pm*-3*n* TaS_3 and $TaSe_3$ at 300 GPa.

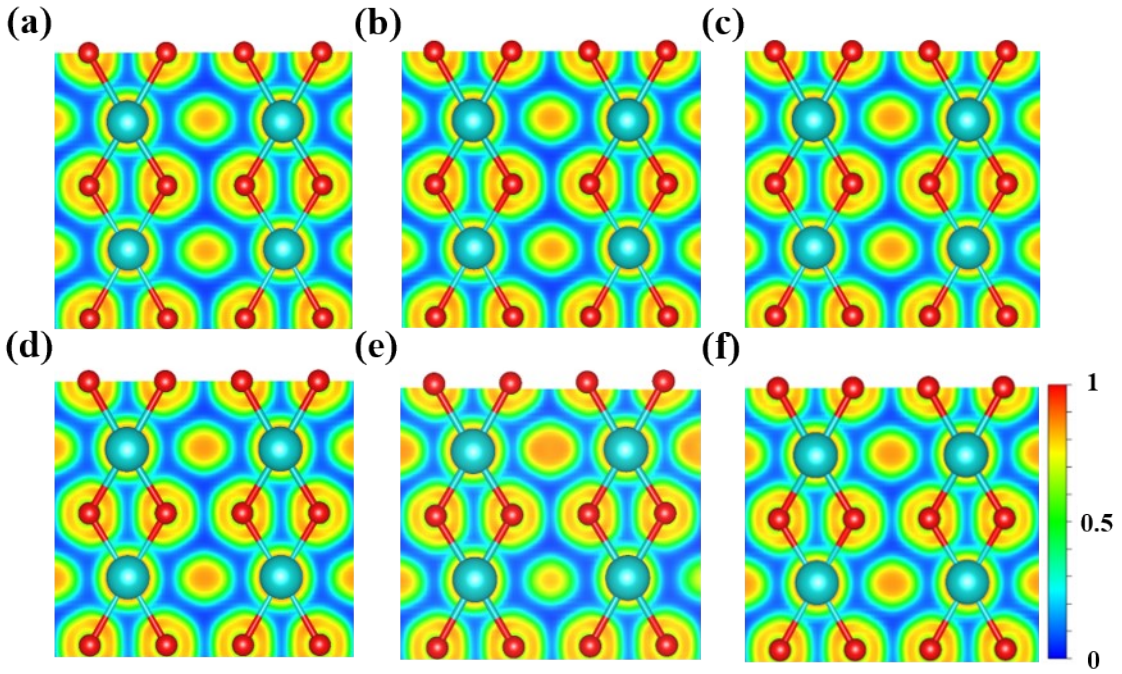

FIG. S16. The ELF maps of *Ibam* Ta_2O_5 at (a) 67, (b) 100, (c) 150, (d) 200, (e) 250, and (f) 300 GPa.

Supporting Tables

Table S1. Structural information of the predicted stable Ta-O phases.

Phases	Pressure (GPa)	Lattice Parameters (Å, °)	Wyckoff Positions (fractional)			
			Atoms	*x*	*y*	*z*
***Imma*-Ta_3O**	50	a = 5.0027	Ta(4c)	0.75000	0.25000	0.25000
		b = 10.5620	Ta(8h)	1.00000	0.47463	0.16367
		c = 7.6646	Ta(8h)	1.00000	0.12020	0.52236
		α = 90.0000	Ta(4e)	0.50000	0.25000	0.57185
		β = 90.0000	O(8g)	0.75000	0.63212	0.25000
		γ = 90.0000				
***P*2_1/*m*-Ta_2O**	100	a= 7.3925	Ta(2e)	0.01819	0.75000	0.74959
		b= 4.1013	Ta(2e)	0.21706	0.75000	0.27122
		c= 4.1773	Ta(2e)	0.54325	0.25000	0.20626
		α = 90.0000	Ta(2e)	0.22286	0.25000	0.77646
		β = 93.7268	O(2e)	0.50295	0.25000	0.68826
		γ = 90.0000	O(2e)	0.26525	0.25000	0.28521
***P*6_3/*mmc*-TaO**	300	a = 2.4558	Ta(2a)	0.00000	0.00000	0.00000
		b = 2.4558	O(2c)	0.66667	0.33333	0.75000
		c = 5.5351				
		α = 90.0000				
		β = 90.0000				
		γ = 120.000				
***I*4/*mmm*-TaO_2**	200	a = 2.5659	Ta(2a)	0.00000	0.00000	0.00000
		b = 2.5659	O(4e)	0.50000	0.50000	0.16272
		c = 6.0421				
		α = 90.0000				
		β = 90.0000				
		γ = 90.0000				
***Ibam*-Ta_2O_5**	100	a = 4.9098	Ta(8j)	0.25608	0.87894	0.00000
		b = 9.7882	O(8j)	0.65119	0.91899	0.00000
		c = 4.2508	O(4a)	0.00000	0.00000	0.75000
		α = 90.0000	O(8g)	0.00000	0.76530	0.75000
		β = 90.0000				
		γ = 90.0000				
***Pm*-3*n*-TaO_3**	300	a=3.6504	Ta(2a)	0.00000	0.00000	0.00000
		b=3.6504	O(6c)	0.00000	0.50000	0.75000
		c=3.6504				
		α = 90.0000				
		β = 90.0000				
		γ = 90.0000				

Table S2. The calculated Löwdin and Mulliken charge transfer amount of Ta and O atoms in the Ta-O phases.

Phases	Pressure (GPa)	Atoms	Mulliken(e)	Löwdin (e)
***Imma*-Ta_3O**	50	Ta1	-0.07	-0.02
		Ta2	0.26	0.22
		Ta3	0.36	0.27
		Ta4	0.63	0.49
		O1	-0.89	-0.73
***P*2_1/*m*-Ta_2O**	100	Ta1	0.06	0.07
		Ta2	0.38	0.27
		Ta3	0.44	0.32
		Ta4	0.78	0.55
		O1	-0.82	-0.60
		O2	-0.84	-0.62
***P*6_3/*mmc*-TaO**	300	Ta1	0.78	0.50
		O1	-0.78	-0.50
***I*4/*mmm*-TaO_2**	200	Ta1	1.56	1.22
		O1	-0.78	-0.61
***Ibam*-Ta_2O_5**	100	Ta1	2.09	1.73
		O1	-0.85	-0.71
		O2	-0.84	-0.70
		O3	-0.80	-0.65
***Pm*-3*n*-TaO_3**	200	Ta1	1.87	1.54
		O1	-0.62	-0.51

Table S3. Bader charge transfer amount of Ta and O atoms in the Ta-O phases.

Phases – bader	Pressure (GPa)	Atoms	Charege(e)
***Imma*-Ta_3O**	50	Ta1	-0.09
		Ta2	0.43
		Ta3	0.54
		Ta4	0.80
		O1	-1.32
***P*2_1/*m*-Ta_2O**	100	Ta1	0.25
		Ta2	0.60
		Ta3	0.67
		Ta4	1.10
		O1	-1.30
		O2	-1.32
***P*6_3/*mmc*-TaO**	300	Ta1	1.28
		O1	-1.28
***I*4/*mmm*-TaO_2**	200	Ta1	2.27
		O1	-1.13
***Ibam*-Ta_2O_5**	100	Ta1	2.87
		O1	-1.12
		O2	-1.15
		O3	-1.16
***Pm*-3*n*-TaO_3**	200	Ta1	2.86
		O1	-0.95

Table S4. Superconducting properties of the metallic Ta-O phases.

Phases	Pressure (GPa)	λ	ω_{log} (K)	T_c (K)
***Pm*-3*n*-TaO_3**	50	1.16	105.01	9.02
***Pm*-3*n*-TaO_3**	100	0.71	207.97	7.53
***Pm*-3*n*-TaO_3**	150	0.56	278.76	5.24
***Pm*-3*n*-TaO_3**	200	0.50	331.41	3.87
***Pm*-3*n*-TaO_3**	250	0.47	364.54	3.26
***Pm*-3*n*-TaO_3**	300	0.44	394.39	2.78
***I*4/*mmm*-TaO_2**	200	0.32	429.22	0.35
***P*6$_3$/*mmc*-TaO**	300	0.24	520.69	0.01
***P*2$_1$/*m*-Ta_2O**	100	0.30	293.93	0.13

Table S5. Bader charge transfer amount of *Pm*-3*n* TaX_3 (*X* = O, S, Se) at 300 GPa.

Phases	Atoms	Charege(e)
***Pm*-3*n*-TaO_3**	Ta	2.89
	O	-0.97
***Pm*-3*n*-TaS_3**	Ta	1.58
	O	-0.53
***Pm*-3*n*-$TaSe_3$**	Ta	1.20
	O	-0.40

References

1. Y. Wang, J. Lv, L. Zhu and Y. Ma, *Phys. Rev. B*, 2010, **82**, 094116.
2. Y. Wang, J. Lv, L. Zhu and Y. Ma, *Comput. Phys. Commun.*, 2012, **183**, 2063-2070.
3. G. Kresse and J. Furthmüller, *Phys. Rev. B*, 1996, **54**, 11169-11186.
4. J. P. Perdew, J. A. Chevary, S. H. Vosko, K. A. Jackson, M. R. Pederson, D. J. Singh and C. Fiolhais, *Phys. Rev. B*, 1992, **46**, 6671-6687.
5. P. Blaha, K. Schwarz, P. Sorantin and S. B. Trickey, *Comput. Phys. Commun.*, 1990, **59**, 399-415.
6. P. Giannozzi, S. Baroni, N. Bonini, M. Calandra, R. Car, C. Cavazzoni, D. Ceresoli, G. L. Chiarotti, M. Cococcioni, I. Dabo, A. Dal Corso, S. de Gironcoli, S. Fabris, G. Fratesi, R. Gebauer, U. Gerstmann, C. Gougoussis, A. Kokalj, M. Lazzeri, L. Martin-Samos, N. Marzari, F. Mauri, R. Mazzarello, S. Paolini, A. Pasquarello, L. Paulatto, C. Sbraccia, S. Scandolo, G. Sclauzero, A. P. Seitsonen, A. Smogunov, P. Umari and R. M. Wentzcovitch, *J. Phys.: Condens. Matter*, 2009, **21**, 395502.
7. L. N. Oliveira, E. K. U. Gross and W. Kohn, *Phys. Rev. Lett.*, 1988, **60**, 2430-2433.
8. M. Lüders, M. A. L. Marques, N. N. Lathiotakis, A. Floris, G. Profeta, L. Fast, A. Continenza, S. Massidda and E. K. U. Gross, *Phys. Rev. B*, 2005, **72**, 024545.
9. M. A. L. Marques, M. Lüders, N. N. Lathiotakis, G. Profeta, A. Floris, L. Fast, A. Continenza, E. K. U. Gross and S. Massidda, *Phys. Rev. B*, 2005, **72**, 024546.
10. P. B. Allen and B. Mitrovic, *Solid State Phys.*, 1982, **37**, 1-92.
11. J. P. Carbotte, *Rev. Mod. Phys.*, 1990, **62**, 1027-1157.
12. I. P. Zibrov, V. P. Filonenko, M. Sundberg and P. E. Werner, *Acta Crystallogr. Sect. B: Struct. Sci.*, 2000, **56**, 659-665.
13. J. H. Yuan, K. H. Xue, Q. Chen, L. R. C. Fonseca and X. S. Miao, *Ann. Phys.*, 2019, **531**, 1800524.
14. I. E. Grey, W. G. Mumme and R. S. Roth, *J. Solid State Chem.*, 2005, **178**, 3308-3314.
15. A. Fukumoto and K. Miwa, *Phys. Rev. B*, 1997, **55**, 11155-11160.
16. S. H. Lee, J. Kim, S. J. Kim, S. Kim and G. S. Park, *Phys. Rev. Lett.*, 2013, **110**, 235502.
17. L. A. Aleshina and S. V. Loginova, *Crystallogr. Rep.*, 2002, **47**, 415-419.
18. R. Ramprasad, *J. Appl. Phys.*, 2003, **94**, 5609-5612.
19. A. Jain, S. P. Ong, G. Hautier, W. Chen, W. D. Richards, S. Dacek, S. Cholia, D. Gunter, D. Skinner, G. Ceder and K. A. Persson, *APL Materials*, 2013, **1**, 011002.